

# Modified Two Switch Flyback topology with an Active Clamp Converter for solar PV micro-inverter application

Rico-Secades Manuel<sup>1</sup>, Quintana-Barcia Pablo<sup>1</sup>, Ribas Javier<sup>1</sup>, Calleja Antonio-Javier<sup>1</sup>, Lopez-Corominas, Emilio<sup>1</sup> and Chinchero Hector<sup>1</sup>

<sup>1</sup> Department of Electrical, Electronics, Communications and Systems (DIEECS)  
 Polytechnics Engineering School of Gijon (EPI-GIJON), Oviedo University  
 Campus of Gijon, 33204 Gijon-Asturias (Spain)  
 Phone/Fax number: +0034 985 182070

**Abstract.** Micro-inverters are one of the many solutions to inject PV energy into the grid. They are usually composed of two stages: a first DC-DC stage that allows performing the MPPT (Maximum Power Point Tracking) function, adding galvanic isolation and raising the voltage to ease the operation of a second stage, the solar Grid Tie Inverter. An interesting and attractive proposal for this first stage is the Flyback converter due to simplicity, isolation, and few components, among others. Unfortunately, for power ratings of 400 W and higher, the problems arising from the leakage inductance of the transformer make it unfeasible. A modification of this converter is the so-called Two-Switch Flyback (TSF). By means of extra components, energy normally lost in this leakage inductance is recirculated to the input. However, the design region becomes narrower, making it difficult to be used in some applications like in an MPPT. This work proposes a modification of TSF by incorporating an auxiliary DC-DC converter denoted as Active Clamp Converter (ACC). This modification of the original TSF allows recovering the energy from the leakage inductance and sending it to the output of the converter, thus avoiding energy recirculation. The proposed topology, with the modification introduced, is a novel solution which improves the efficiency compared to the classical TSF stage.

**Key words.** Micro-inverter, Maximum Power Point Tracking (MPPT), Two-Switch Flyback (TSF), PV-solar panel, Active Clamp Converter (ACC).

## 1. Introduction

The use of grid-tie micro-inverters for a single solar photovoltaic module is a hot topic of great practical interest [1]–[5]. In addition, the power capability of PV solar modules is constantly growing and power exceeding 400 W is now common in the market [6]. Fig. 1 shows the typical structure of a two-stage solar micro-inverter, consisting of a high step-up DC-to-DC converter with galvanic isolation stage followed by a grid-tie inverter (GTI) stage. The DC-to-DC stage will be in charge, at each instant, of obtaining the maximum possible energy from the solar panel, implementing a maximum power point tracking (MPPT) philosophy. The power is delivered to a DC bus with a suitable high voltage (in the figure 400 V). While the inverter stage will be in charge of maintaining the high DC voltage bus ( $V_{bus}$ ) at a stable value, evacuating the generated energy to the power grid. This work focuses on the MPPT stage and the paper proposes a new power conversion stage derived from the Flyback DC-to-DC converter that presents a number of important advantages.

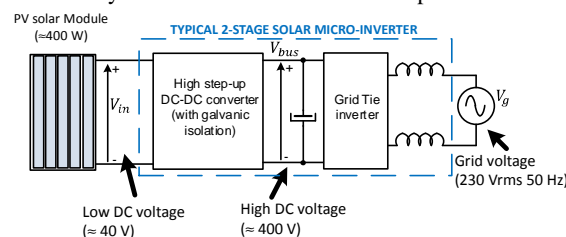


Fig. 1 Typical 2-stage solar micro-inverter.

Fig. 2 shows a Flyback DC-to-DC converter used as the MPPT stage for a single PV solar module. This power stage is very interesting for this application: a single control signal, a single power MOS transistor, galvanic isolation and simplicity. However, there is an important disadvantage: its poor efficiency derived from losses caused by leakage inductance ( $L_k$ ) [7]. This means that for power ratings above 400 W this is not a viable stage [8].

A new topology has been proposed to solve this problem: The Two-Switch Flyback (TSF) converter [9]–[12]. This converter maintains a single control signal that acts simultaneously over the two power MOS transistors (T1L and T2H). Basically, the operation of the TSF converter is identical to the classic Flyback converter, with an important advantage, the TSF allows the energy stored in the leakage inductance ( $L_k$ ) to be recovered to the input voltage instead of being dissipated (snubber), as in the original Flyback converter.

The price to pay is the inclusion of one MOS transistor and two diodes additional and introducing limitations in the operating range of the converter. The Fig. 3 shows the TSF converter used at MPPT stage. Several references discuss this converter for different applications, one of them being the use as a DC-to-DC stage for MPPT applications.

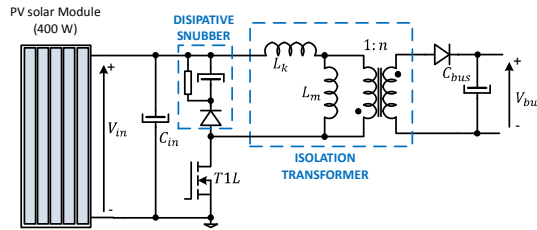


Fig. 2 High step-up DC-to-DC stage based on a classical Flyback converter.

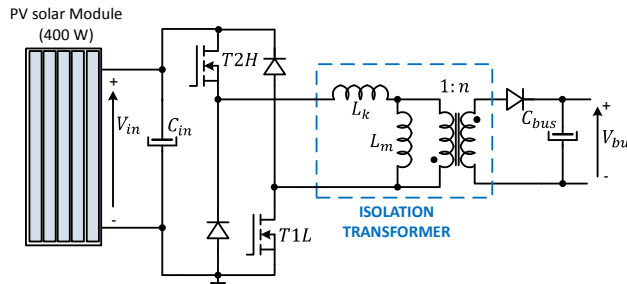


Fig. 3 High step-up DC-to-DC stage based on the Two-Switch Flyback (TSF) converter.

At this point, the proposal of this work is shown in Fig. 4. A small DC-to-DC converter (Flyback converter in the figure) is introduced to recover the energy from the leakage inductance, delivering this energy directly to the output and thus avoiding energy recirculation.

This small auxiliary converter is denoted in this work as Active Clamp Converter (ACC). This ACC is designed to maintain a constant voltage at its input ( $V_{clamp}$ ) which is generated from the energy recovered and collected on a storage capacitor ( $C_{clamp}$ ). The operation of the TSF with ACC is identical to the original TSF, with three major advantages:

- (1) The aforementioned delivery of the recovered energy directly to the outlet without energy recirculation.
- (2) The flexibility to select the value of the clamp voltage ( $V_{clamp}$ ), allowing extending the operating range of the converter and facilitating the correct operation of all design conditions.
- (3) A single ACC can be shared among several TSFs in case of interleaving, significantly improving the performance of the whole. This is a topic for future work.

Note that if the TSF were designed with ACC with a clamp voltage ( $V_{clamp}$ ) equal to the input voltage ( $V_{in}$ ), the operation would be similar to the original TSF (without energy recirculation). The proposal has the additional advantage of being compatible with interleaving strategies, where several TSFs can share a single ACC. This interesting option will be presented in future works.

The ACC element can be easily implemented using any DC-to-DC stage with galvanic isolation. In this work, a classical small Flyback converter is proposed to implement this additional element.

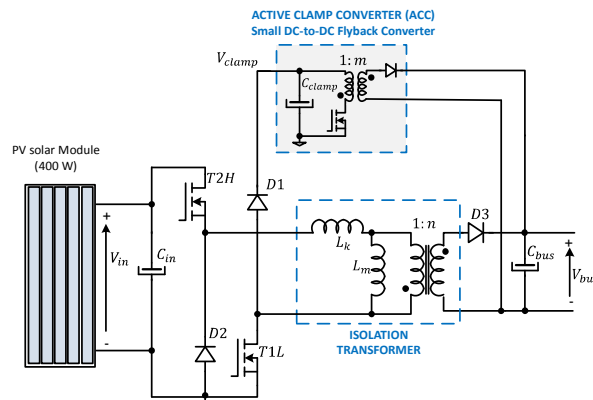


Fig. 4 High step-up DC-to-DC stage based on a modified Two-Switch Flyback (TSF) converter with an Active Clamp Converter (ACC) implemented with a small power DC-to-DC Flyback Converter.

## 2. Analysis in steady-state operation

In order to proceed with the analysis of the proposed topology in a simple and understandable way, a simplified representation of the topology is used. Fig. 5 shows this simplified representation of the TSF with ACC to obtain basic equations and waveforms in steady-state operation. The PV solar module has been represented with a current source ( $i_p$ ) the high DC bus voltage by means on a battery ( $V_{bus}$ )

and the ACC be means of its Thevenin equivalent. The ACC input voltage or clamp voltage is denoted as  $V_{clamp}$  and the output part is shown as a current source that delivers to the output the energy recovered from the leakage inductance ( $P_{clamp}$ ).

The power topology consists of two power MOS transistors (T2H and T1L), which are driven by the same control signal. An additional letter H or L has been added to the name of the MOS transistors to indicate simple control (low side) or more complex or floating control (high side). The output bus has been represented as a stable voltage ( $V_{bus}$ ) since the responsibility for the correct stabilization of this voltage corresponds to the subsequent stages (in this case, the GTI).

The isolation transformer has been represented by means of an ideal transformer to which the magnetizing inductance ( $L_m$ ), its resistive losses ( $R_s$ ) and leakage inductance ( $L_k$ ) have been added. The analysis will obviously consider the effect of the transformer leakage inductance, unlike other analyses [2] with the TSF that do not take it into account. The steady-state operation of this converter has four stages: two when the two transistors are ON (denoted as ON1 and ON2) and other two when the two transistors are OFF (denoted as OFF1 and OFF2).

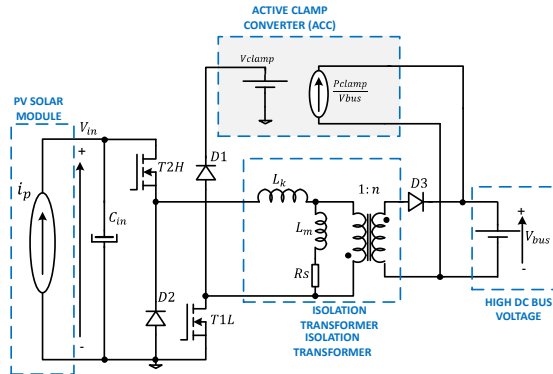


Fig. 5 Simplified representation of TSF with ACC for analysis operation.

During the ON1 stage (shown in Fig. 6), the two transistors (T2H and T1L) are in conduction. The current through the leakage inductance ( $L_k$ ) starts at zero and therefore also that of both MOS transistors.

Diode D3 will remain in conduction during this interval, until the current in the leakage inductance ( $i_{Lk}$ ) reaches the magnetizing current ( $i_{Lm}$ ). The current in D3 decreases smoothly to zero during this interval.

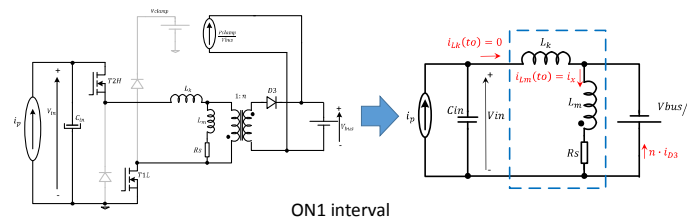


Fig. 6 Equivalent circuit during ON1 interval (T2H, T1L and D3 are ON).

Equations during ON1 interval:

$$V_{in} + \frac{V_{bus}}{n} = L_k \cdot \frac{di_{Lk}}{dt} \tag{1}$$

$$-\frac{V_{bus}}{n} = L_m \cdot \frac{di_{Lm}}{dt} + R_s \cdot i_{Lm} \tag{2}$$

$$i_p - i_{Lk} = C_{in} \cdot \frac{dV_{in}}{dt} \tag{3}$$

$$n \cdot i_{D3} = i_{Lm} - i_{Lk} \tag{4}$$

ON1 initial conditions ( $t_0$ ):

$$i_{Lk}(t_0) = 0$$

$$i_{Lm}(t_0) = i_x$$

ON1 final conditions ( $t_1$ ):

$$i_{Lk}(t_1) = i_{Lm}(t_1) = i_o$$

During ON2 interval, (see Fig. 7), the two MOS transistors remain conducting, while the output diode D3 does not (its current has reached zero). The magnetizing and leakage inductances are powered in series from the input. The end of the interval ( $t_2$ ) coincides with the end of the excitation time of the transistors, reaching in both inductors the maximum current value ( $i_m$ ).

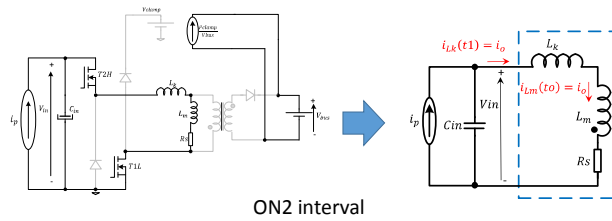


Fig. 7 Equivalent circuit during ON2 interval (T2H and T1L are ON and D3 is OFF).

Equations during ON2 interval:

$$V_{in} = L_k \cdot \frac{di_{Lm}}{dt} + L_m \cdot \frac{di_{Lm}}{dt} + R_S \cdot i_{Lm} \quad (5)$$

$$i_p - i_{Lm} = C_{in} \cdot \frac{dV_{in}}{dt} \quad (6)$$

$$i_{Lk} = i_{Lm} \quad (7)$$

$$i_{D3} = 0 \quad (8)$$

ON2 initial conditions (t1):

$$i_{Lm}(t1) = i_{Lk}(t1) = i_o$$

ON2 final conditions (t2):

$$i_{Lk}(t2) = i_{Lm}(t2) = i_m$$

$$t2 - t1 = d \cdot T$$

The third interval (OFF1) starts with the simultaneous switch-off order in the two power MOS switches (see Fig. 8). Diode D3 and diodes D1 and D2 goes into conduction immediately. Diodes D1 and D2 will be in conduction for the duration of the demagnetization of the transformer's leakage inductance ( $L_k$ ). Thus, the energy stored in this inductance ( $L_k$ ) is transferred to the output through the ACC. This stage OFF1 is the main novelty and originality of this converter, introducing the new design parameter ( $V_{clamp}$ ) that introduces flexibility and notably widens the converter's working region. The efficiency of the converter is significantly increased by being able to recover all this normally lost energy and avoid unnecessary energy recirculation.

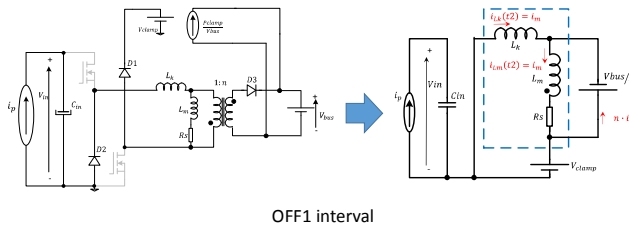


Fig. 8 Equivalent circuit during OFF1 interval (T2H and T1L are OFF and D3 is ON).

Equations during OFF1 interval:

$$\frac{V_{bus}}{n} - V_{clamp} = L_k \cdot \frac{di_{Lk}}{dt} \quad (9)$$

$$-\frac{V_{bus}}{n} = L_m \cdot \frac{di_{Lm}}{dt} + R_S \cdot i_{Lm} \quad (10)$$

$$i_p = C_{in} \cdot \frac{dV_{in}}{dt} \quad (11)$$

$$n \cdot i_{D3} = i_{Lm} - i_{Lk} \quad (12)$$

OFF1 initial conditions (t2):

$$i_{Lm}(t2) = i_{Lk}(t2) = i_m$$

OFF1 final conditions (t3):

$$i_{Lk}(t3) = 0$$

$$i_{Lm}(t3) = i_y$$

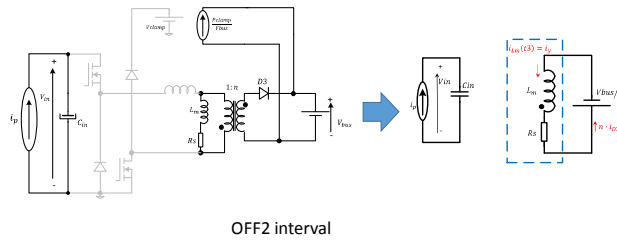


Fig. 9 Equivalent circuit during OFF2 interval (T2H and T1L are OFF and D3 is ON).

Finally, the OFF2 interval completes a switching cycle in steady state of the converter (see Fig. 9). This last interval is completely similar to that one on a conventional Flyback converter, with only the output diode (D3) remaining in conduction. Equations during this last interval are:

$$i_{Lk} = 0 \quad (13)$$

$$-\frac{V_{bus}}{n} = L_m \cdot \frac{di_{Lm}}{dt} + R_s \cdot i_{Lm} \quad (14)$$

$$i_p = C_{in} \cdot \frac{dV_{in}}{dt} \quad (15)$$

$$n \cdot i_{D3} = i_{Lm} \quad (16)$$

OFF2 initial conditions (t3):

$$i_{Lk}(t3) = 0$$

$$i_{Lm}(t3) = i_y$$

OFF2 final conditions (t4):

$$i_{Lk}(t4) = 0$$

$$i_{Lm}(t4) = i_x$$

Obviously, the interval (t4-to) is the switching period and the intervals (t2-to) and (t4-t2) are ON and OFF switching intervals respectively.

$$t4 - t_o = T \quad (17)$$

$$t4 - t2 = (1 - d) \cdot T \quad (18)$$

$$t2 - t_o = d \cdot T \quad (19)$$

The Fig. 10 summarizes the basic waveforms in steady-state operation during the four intervals, emphasizing in red color the two intervals (ON1 and OFF1) where the magnetization and demagnetization of the leakage inductance differ from the classical Flyback converter. For each operating point, the average current through the transistors represents the average current obtained from the solar panel:

$$(i_p)_{avg} = (i_{T1L})_{avg} = (i_{T2H})_{avg}$$

### 3. Design example and simulation results

Using the Fig. 4 as a reference, the design of an MPPT stage for a 380 W solar panel has been proposed, so that it delivers the generated power over a DC bus, which is assumed to be stabilized at 400 V. A monocrystalline solar module from ERA solar (72 cells Mono PERC technology) was used for evaluation, specifically model ESPSC 380M. Its main parameters under STC conditions are as follows:

- MPP voltage = 40.5 V
- MPP current = 9.39 A
- MPP power = 380 W
- Open Circuit Voltage = 48.9 V
- Short Circuit Current = 9.75 A
- Module efficiency = 19.16 %

The solar module has been modeled using the free software LTspice and has been simulated in STC conditions (Irradiance 1000 W/m<sup>2</sup> and temperature 25 °C). The data used for the design and simulation of the TSF with ACC are as follows:

- Output voltage Vbus = 400 V
- Switching Frequency Fs = 20 kHz
- Transformer turn-ratio 1:10 (n=10)
- Magnetizing Inductance Lm = 1 mH

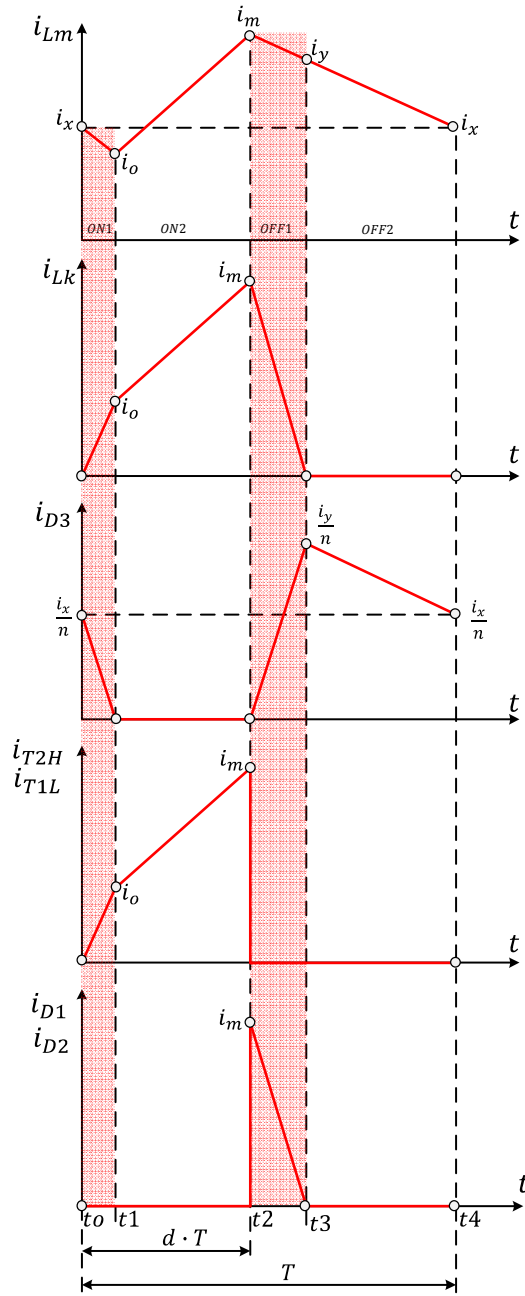


Fig. 10 Main waveforms in steady-state operation.

- Leakage Inductance  $L_k = 5\% L_m$
- Clamp Voltage in the ACC  $V_{clamp} = 200 \text{ V}$
- Input capacitor  $C_{IN} = 470 \mu\text{F}$

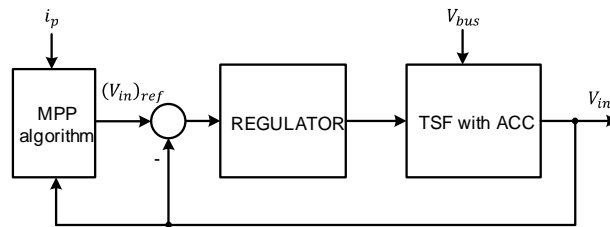


Fig. 11 Control structure to use TSF with ACC as MPPT stage.

Only for topology evaluation purposes, Fig. 11 shows the strategy will be implemented to regulate the input voltage ( $V_{IN}$ ) and subsequently implement MPPT algorithm. The objective of the MPPT algorithm will be to perform an active search for  $V_{IN}$  voltage so that the panel works at its maximum voltage point (Perturb, Wait and Observe – PWO algorithm have been implemented). In STC conditions, this voltage should be 40.5 V for the ESPSC 380M solar panel used in the design.

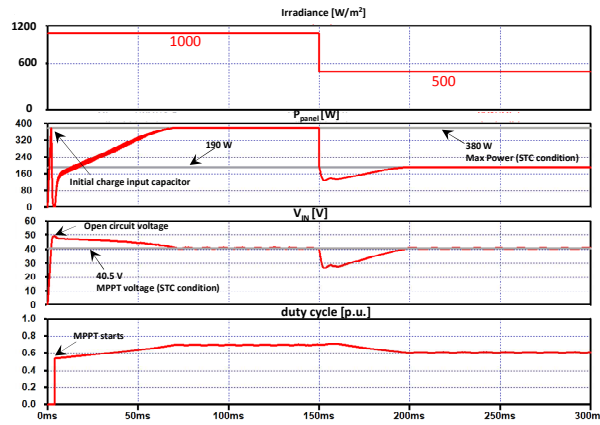


Fig. 12 Detail of MPPT algorithm implemented for topology validation (Perturb, Wait and Observe – PWO)

The Fig. 12 shows the operation detail of the well-known Perturb, Wait and Observe (PWO) algorithm implemented with irradiance 1000 W/m<sup>2</sup> and with irradiance 500 W/m<sup>2</sup>, details of algorithm implementation are not included in this work and it has been implemented only to validate the new proposed topology. The well-known PWO algorithm is not the goal of this work.

A delay in the start of operation of the MPPT algorithm of 4 mS has been introduced to allow time for the correct charging of the input capacitor ( $C_{IN}$ ), as shown in the waveforms (duty cycle remains to zero during this initial interval).

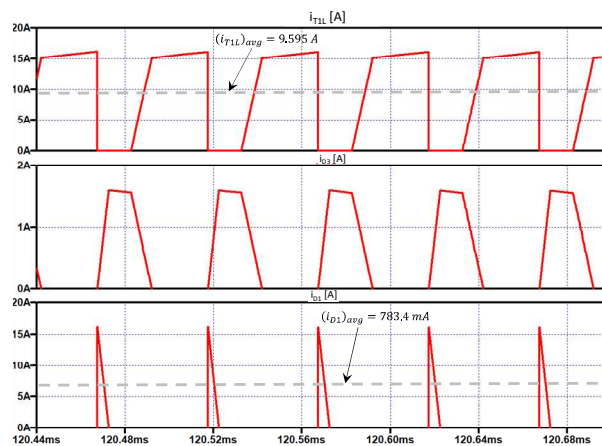


Fig. 13 Detail of current in diodes and MOS switches in MPPT point (380 W).

The Fig. 13 shows the main current waveforms in the diodes and MOS switches of the circuit, obtained at the MPP point on the PV-panel (380 W). According theoretical equations, it can be seen how during the ON1 interval, both MOS transistors enter in conduction at zero current (zero turn-on switching losses). Gradually its current is increasing and consequently reducing the current in the output diode (D3).

Then, the turn-off process of the output diode (D3) is soft, drastically reducing the effects of recovery time on the conduction output of this diode. This is one of the main effects of the leakage inductance used in advantage in the proposed topology. Highlight the energy recovered through diodes D1 and D2, which presents an average value of 783.4 mA. Considering the clamp voltage ( $V_{clamp}$ ) of 200 V used in the design, this means an average power of 156 W has been recovered through the ACC module.

For comparison, a traditional Flyback converter used as MPPT stage handling the power of 380 W and with these losses due to the large leakage inductance (156 W) would be totally unfeasible and unthinkable. However, the incorporation of this auxiliary ACC converter, allows recovering this energy and significantly improving the conversion efficiency in spite of the large leakage inductance in the isolation transformer. Hotwithstanding, the smaller the dispersion inductance, the less energy it will need to handle in this auxiliary ACC converter and the higher the overall efficiency will be. The addition of these additional elements, the quality of the overall operation of the converter has improved significantly.

#### 4. Conclusion and future works

The modification of the TSF converter by incorporating an auxiliary converter (denoted as ACC), greatly improving the possibilities of using this power stage as the first MPPT stage in a solar grid-tie micro-inverter (solar GTI). The design equations for this new converter in steady state have been established and a new degree of freedom ( $V_{clamp}$ ) is incorporated into the design. The entire systematic design process (design guide), the dynamic modeling of the converter to optimize the regulator design and the details of the implemented MPPT algorithm will be presented in future works. The next step should be to build an experimental laboratory prototype and verify the real efficiency with a practical implementation of the proposed converter.

## Acknowledgement

This work has been sponsored by the Spanish Company Normagrup S.A. and supported by “Ministerio de Economía, Industria y Competitividad” of the Government of Spain under Research Grants MCI-20-PID2019-105568RB-I00 and MCINN-22-TED2021-129372B-I00 and by the Principality of Asturias under Research Grant GR-2010-0010 (CE3I2).

## References

- [1] M. A. Rezaei, K. J. Lee, and A. Q. Huang, “A high efficiency flyback micro-inverter with a new adaptive snubber for photovoltaic applications,” 2015 IEEE Energy Convers. Congr. Expo. ECCE 2015, vol. 31, no. 1, pp. 3308–3313, 2015, doi: 10.1109/ECCE.2015.7310126.
- [2] G. H. Min, K. H. Lee, J. I. Ha, and M. H. Kim, “Design and Control of Single-Phase Grid-Connected Photovoltaic Microinverter with Reactive Power Support Capability,” 2018 Int. Power Electron. Conf. IPEC-Niigata - ECCE Asia 2018, pp. 2500–2504, 2018, doi: 10.23919/IPEC.2018.8507578.
- [3] D. Lopez, F. Flores-Bahamonde, H. Renaudineau, and S. Kouro, “Double voltage step-up photovoltaic microinverter,” Proc. IEEE Int. Conf. Ind. Technol., pp. 406–411, 2017, doi: 10.1109/ICIT.2017.7913265.
- [4] S. S. Converter and S. Inverter, “Highly Efficient Microinverter With,” IEEE Trans. Ind. Electron., vol. 62, no. 6, pp. 3516–3523, 2015.
- [5] M. Pisano, F. Bizzarri, A. Brambilla, G. Gruosso, and G. S. Gajani, “Micro-inverter for solar power generation,” SPEEDAM 2012 - 21st Int. Symp. Power Electron. Electr. Drives, Autom. Motion, pp. 109–113, 2012, doi: 10.1109/SPEEDAM.2012.6264547.
- [6] B. G. Bhang, W. Lee, G. G. Kim, J. H. Choi, S. Y. Park, and H. K. Ahn, “Power Performance of Bifacial c-Si PV Modules with Different Shading Ratios,” IEEE J. Photovoltaics, vol. 9, no. 5, pp. 1413–1420, 2019, doi: 10.1109/JPHOTOV.2019.2928461.
- [7] A. Abramovitz, C. S. Liao, and K. Smedley, “State-plane analysis of regenerative Snubber for Flyback converters,” IEEE Trans. Power Electron., vol. 28, no. 11, pp. 5323–5332, 2013, doi: 10.1109/TPEL.2013.2243845.
- [8] A. Mukherjee, M. Pahlevaninezhad, and G. Moschopoulos, “A passive snubber circuit for flyback microinverters in solar energy systems,” Conf. Proc. - IEEE Appl. Power Electron. Conf. Expo. - APEC, pp. 3236–3240, 2013, doi: 10.1109/APEC.2013.6520763.
- [9] C. W. Lin and Y. Y. Tzou, “Digital primary-side sensing and PFC control of a flyback converter,” IEEE Energy Convers. Congr. Expo. Energy Convers. Innov. a Clean Energy Futur. ECCE 2011, Proc., pp. 2603–2608, 2011, doi: 10.1109/ECCE.2011.6064116.
- [10] A. Al Mamun, M. I. I. Sakib, K. F. I. Faruque, M. R. Uddin, and K. M. Salim, “A Grid-Tie Microinverter Design Based on Dual-Switch Flyback Topology for Solar PV Application,” 8th Int. Conf. Eng. Emerg. Technol. ICEET 2022, no. October, pp. 27–28, 2022, doi: 10.1109/ICEET56468.2022.10007209.
- [11] H. Choi, “Two-switch BCM flyback single-stage PFC for HB LED lighting applications,” Conf. Proc. - IEEE Appl. Power Electron. Conf. Expo. - APEC, pp. 3125–3130, 2013, doi: 10.1109/APEC.2013.6520747.
- [12] M. G. Kim and Y. S. Jung, “A novel soft-switching two-switch flyback converter with a wide operating range and regenerative clamping,” J. Power Electron., vol. 9, no. 5, pp. 772–780, 2009.